Multi-scale relaxation in aging gels: from localized plastic events to system-spanning 'quakes'

Zeno Filiberti,* Roberto Piazza, and Stefano Buzzaccaro†
Department of Chemistry, Materials Science, and Chemical Engineering (CMIC), Politecnico di Milano, Edificio 6, Piazza Leonardo da Vinci 32, 20133 Milano, Italy
(Dated: July 22, 2019)

Relaxation of internal stresses through a cascade of microscopic restructuring events is the hallmark of many materials, ranging from amorphous solids like glasses and gels to geological structures subjected to a persistent external load. By means of Photon Correlation Imaging, a recently developed technique that blends the powers of scattering and imaging, we provide a spatially and temporally resolved survey of the restructuring and aging processes that spontaneously occur in physical gels originating from an arrested phase separation. We show that the temporal dynamics is characterized by an intermittent sequence of spatially–localized 'micro-quakes' that eventually lead to global rearrangements occurring at a rate that scales with the gel age. Notably, these dramatic upheavals of the gel structure are heralded by a progressive acceleration of the microscopic gel dynamics that originates from recognizable active spots and then spreads at a large but finite speed through the gel. Within the 'slack' phase between two of these 'macro–quakes', the fluctuations of the degree of temporal correlation obey a non-Gaussian statistics described by a generalized logistic distribution. The evidence we obtained bear consistent analogies with the stress relaxation processes taking place in earthquake sequences and with the intermittent restructuring of plastic crystals at the microscale.

Structural relaxation in soft disordered solids like colloidal gels is a topic of long-standing interest, both in consideration of the growing number of applications of these systems and because of their basic interest [1–6]. However, relating the macroscopic mechanical and rheological behavior of these materials to their spontaneous restructuring processes, which involve a broad range of time, energy, and length scales, is still challenging [7–14]. To complicate matters further, the microscopic structure and dynamics of these disordered networks display a slow and heterogeneous evolution in time [2, 6, 15–18] that consistently affects their macroscopic mechanical response [17]. For instance the time evolution of the strain in soft materials subjected to a constant load can be 'jagged' [19, 20], i.e., these systems do not deform smoothly but rather through a series of swift finite rearrangements. These intermittent events, usually dubbed as plastic avalanches or 'quakes', are observed not only in soft materials like dense colloids [21], foams [20], gels [7, 22, 23], and granular fluids [24], but also in hard amorphous materials such as porous glasses [25], wood [26] paper [27] metal microcrystals [28] and glasses [29, 30].

Notwithstanding their diverse mechanisms of deformation, all these structures share a rugged energy landscape and a temporally–heterogeneous dynamics. As a consequence, the statistics and dynamics of their structural rearrangements events can often be described by similar models of plastic deformation [19, 31]. Among them, elastoplastic models (EPMs) relying on simple and very general assumptions can be profitably exploited to bridge the manifold length scales leading from the microscopic restructuring events to the overall macroscopic behavior [19]. EPMs handle the material as a collection of mesoscopic blocks whose elastic response turns into a plastic relaxation when the load they are subjected to exceed a given threshold. These localized relaxations redistribute stresses in the system and are likely to trigger further rearrangements at a distance, hence creating plastic avalanches that account for the occurrence of nonlocal effects in the flow of disordered solids [14, 17, 19, 31]. In colloidal gels the large size of the constituent particles and the interaction strength, often comparable to k_BT, make the structure quite sensitive to thermal fluctuations. Hence this 'cascade' of plastic events not only affects the mechanical response of the material to external stresses, but also leads to spontaneous aging of its mechanical properties driven by thermally activated processes [32, 33].

Detecting individual plastic rearrangements and monitoring how this restructuring events spread over large distances with long-ranged spatial correlations is a challenging experimental task. To this end, both Dynamic Light Scattering (DLS) and Optical Microscopy (OM), two favourite optical methods for investigating soft materials, suffer from opposite drawbacks [34]. DLS provides us with detailed information on the microscopic dynamics of particles and structures down to the nanoscale, but it lacks spatial resolution. Per contra, OM methods allow us to resolve spatially heterogeneous structures and to track particle motion in real space, but the spatial scales they probe are bounded from below by the resolution limit and, from above, by the limited field

* Current address:Dipartimento di Scienza e Alta Tecnologia, Università dell'Insubria, Via Valleggio 11, 22100 Como, Italy
† stefano.buzzaccaro@polimi.it

of view of a microscope. Nevertheless, recent advancements in optical correlation methods show that there are ways to probe the microscopic dynamics by operating in the Fourier space and measuring time-correlation functions like in DLS, still retaining the spatial resolution of OM [22, 35–37]. By investigating a model system of particles whose interactions can accurately be tuned with temperature, we plan to show that the application of these novel optical correlation techniques unravels an extremely rich scenario for the restructuring processes, characterized by a complex multi-scale aging dynamics, taking place in a colloidal gel over a surprisingly long period of time. Such a complex temporal evolution, suggests a strong connection with stress relaxation in cyclic earthquake sequences [38, 39], and with recently proposed self-organized oscillator mechanism in crystal plasticity [28].

This paper is organized as follows. In Section I, we first introduce the investigated colloidal systems, discuss its phase diagram, and pinpoint the specific route to gelation we selected. We then describe Photon Correlation Imaging, the optical correlation technique we used, showing that it can be exploited as a unique tool to obtain a detailed description of the temporally intermittent and spatially heterogenous dynamic processes taking place in a disordered colloidal solid.

After a preliminary description of the gelation process and of the initial gravity settling of the gel into a mechanical stable structure, Section II is devoted to the detailed analysis of the dynamical effects by which the nonequilibrium gel structure relaxes and renovates, progressively releasing its frozen-in internal stresses. In particular we show that the temporal dynamics is characterized by an intermittent sequence of spatially–localized 'micro-quakes' eventually leading to sudden restructuring events involving the whole gel, which we dub 'macro–quakes'. Notably, these dramatic upheavals of the gel structure are heralded by a 'jittery' phase of the gel dynamics, so that these apparently random events can actually be *predicted*, at least statistically, from the progressive speeding up of the microscopic dynamics.

In Section III we perform a detailed statistical analysis of the local degree of temporal correlation in the gel that provides quantitative bases to the evidence mentioned above. In particular, we show that the fluctuations of the degree of correlation obey a non–Gaussian statistics accurately described by a probability distribution belonging to the class of generalized logistic distributions, while the distribution of the strongest micro–quakes within is in full agreement with the predictions of an Extreme Value Analysis.

In the final discussion (Section IV) we suggest that the complex restructuring and aging processes we detected may be reminiscent of the mechanisms of stress relaxation in earthquake sequences [38, 39] and of recently proposed self-organized oscillator mechanisms in crystal plasticity [28].

I. MATERIALS AND METHODS

A. Colloidal system

Due to their low refractive index contrast with water, particles made of fluorinated polymers are a favourite choice for investigating concentrated aqueous suspensions and are quite promising in many applications too, due to their superior chemical stability and high biological compatibility. So far, most physical investigations have addressed particles made of perfluorinated polymers (copolymers of polytetrafluoroethylene, [40]), whose synthesis requires however complex and dangerous fluorine chemistry. Recently, however, a new synthesis protocol based on a sophisticated form of emulsion polymerization (RAFT, Reversible Addition Chain Transfer) has been engineered [41]. The distinctive aspect of this protocol is that it uses 'macro-surfmers', namely, macromolecular surface-active RAFT agents that substitute standard surfactants in the emulsion polymerization. These macro-surfer are deeply embedded inside the particle with covalent links, but at the same time they provide extremely good particle stabilization by protruding their hydrophilic part out of the surface. The particles used in this work have been synthesized using a neutral surfmer based on a PEGylated methacrylate monomer that provides the particle surface with a covalently–linked stabilizing layer made of short PEG chains. Dynamic light scattering yields a particle radius of $R = 50 \pm 2\,\mathrm{nm}$ with a polydispersity of about 8%, while measurements of the sedimentation velocity as a function of the solvent density ρ_s gives a particle material density $\rho_p = 1.49\,\mathrm{g/cm^3}$. The refractive index n_s of the solvent can easily be matched to the particle refractive index n_p by adding appropriate amounts of 2,2'-thiodiethanol (TDE), a nontoxic liquid with high refractive index ($n_{\mathrm{TDE}} = 1.5215$)) miscible with water in any ratio [42]. Varying the TDE/water ratio allows to obtain an accurate value of the particle refractive index, $n_p = 1.382 \pm 0.002$.

The interparticle interactions between PEG-grafted particles are closely related to the temperature dependence of the solubility of short PEG chains in water [41, 43] that is strongly affected by the presence of electrolytes, an effect which is strongly salt-specific. For instance, a salt like ammonium sulfate weakens the hydrogen bonds between PEG and water, which becomes a marginal solvent for the stabilizing polymer layer turning the effective interparticle forces from repulsive to attractive. In fact, when about 0.6 M of Na_2SO_4 is added to water, our particles show a liquid–liquid phase separation with the solvent. Hence, the particle/solvent system behaves as a critical binary mixture where, however, one of the two components is a huge colloidal object. Because of this large size–asymmetry the colloid, when quenched inside the coexistence gap, does not undergo a full phase separation into the equilibrium phases, but rather gets arrested into an amorphous gel phase that is fully thermo–reversible [44]. Here we will focus our at-

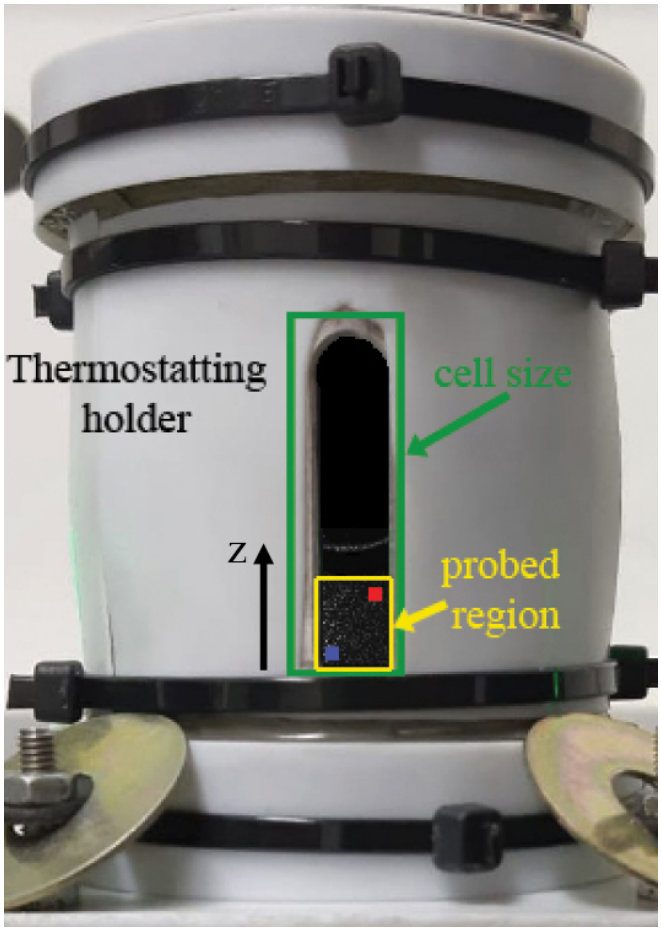

FIG. 1. Thermostatting holder as seen from the detection camera, with the laser sheet impinging upon the cell from the left side. The figure also shows the cell size and the region detected by the PCI camera, together with the 'fast' (red dot) and 'slow' (blue dot) regions discussed in Section II C.

tention on a gel prepared at an initial particle volume fraction $\phi_0 = 0.09$ that shows a gelation temperature $T_{gel} = 43°$ C. We will discuss a gel prepared at $T = 54°$ C (corresponding to a quench depth $T/T_{gel} \simeq 1.035$), which is representative of the aging behaviour of gels obtained for shallow to moderate quenches inside the coexistence region (between 1 and 5% in excess of T_{gel}, approximately).

B. Photon Correlation Imaging

Photon Correlation Imaging (PCI) is a recently introduced optical method, suitable to investigate slow dynamics in colloidal glasses and gels by measuring the time–correlation function of the scattered light, as in standard Dynamic Light Scattering (DLS), but with the major advantage of allowing for spatial resolution by probing the *local* dynamics at distinct points within the scattering volume. We shall give only a summary description of PCI, mainly emphasizing the rich amount of physical information that can be extracted using this powerful technique, and referring to the seminal contributions by L. Cipelletti and coworkers for a more detailed analysis [35]. Basically, the experiment consists in forming on a multi-pixel camera an image of the scattering volume, observed at a given scattering angle ϑ through a suitably stopped-down optics. In other words, the imaging optics is provided with a partially closed iris diaphragm placed in the focal plane of the lens that, besides accurately selecting the scattering wave-vector $q = (4\pi/\lambda)\sin(\vartheta/2)$, causes the image to become 'speckled' because the intensity at each given point on the image plane originates from the interference of the field scattered by a finite–size region in the sample plane. The simultaneous measurement of the time–dynamics over many speckles by the multi–pixel detector, besides providing a fast ensemble averaging of the intensity correlation function (crucial when investigating samples with a very slow dynamics), allows one to identify the occurrence and follow the temporal evolution of those dynamic effects associated to the presence of spatial heterogeneities in the investigated sample. Quantitatively, the latter can be characterized as follows. First, the spackle pattern is subdivided into 'regions of interest' (ROIs) by grouping together a given number of adjacent pixels. Then, one introduces the so-called 'degree of space–time correlation' (or correlation index') $c_I(\tau; t, \mathbf{r})$ between two images taken at times t and $t + \tau$ as

$$c_I(\tau; t, \mathbf{r}) = \frac{\langle I_p(t) I_p(t+\tau) \rangle_{\mathbf{r}}}{\langle I_p(t) \rangle_{\mathbf{r}} \langle I_p(t+\tau) \rangle_{\mathbf{r}}} - 1, \qquad (1)$$

where I_p is the scattered intensity measured by the p-th pixel and $\langle \cdots \rangle_{\mathbf{r}}$ denotes an average over all pixels within a ROI centered around $\mathbf{r}$. Hence, $c_I(\tau; t, \mathbf{r})$ is simply related to the covariance between the intensity measured on the same speckle at two different times, sampled over the given ROI and, in particular, $c_I(0; t, \mathbf{r})$ is the relative variance of the intensity in $\mathbf{r}$ at time t. Note that c_I is a function of the delay time τ that, in samples displaying a restructuring and aging kinetics, depends parametrically on the aging time t (and, for spatially inhomogeneous samples like those we shall consider, also on the local position $\mathbf{r}$). In fact, as we shall see, it is exactly this time-dependence that yields the basic features of the gelation process. Provided that the investigated kinetics is sufficiently slow, however, the statistical accuracy can be enhanced by time–averaging $c_I(\tau; t, \mathbf{r})$ over a time window δt that is much shorter than the characteristic evolution time of the investigated kinetics, which allows reducing the statistical noise due to finite sampling on the limited number of pixels in a ROI. The local dynamics can then be quantified by defining [45]

$$g_2(\tau) - 1 = \langle c_I(\tau; t, \mathbf{r}) \rangle_{\delta t} \,. \qquad (2)$$

Such a 'coarse-grained' correlation index actually bears the same information as the intensity correlation function

measured in a standard DLS experiment, yet with the crucial advantage of a much better statistical accuracy due to pre-averaging over the speckles in a ROI, which allows averaging over a time interval δt much shorter than required in standard DLS measurements. Besides, since PCI is in fact an imaging technique, the measurements the position of the cross-correlation peak between two speckle patterns obtained at different times is directly related to local physical displacements in the sample, like in particle Image Velocimetry (PIV) [36, 37]. The amplitude of the correlation peak, moreover, decays on the time scale of the local rearrangement dynamics, allowing one to set apart the spurious contribution to the decay of the correlation function due to the overall translation of the speckle pattern.

In our setup the sample, illuminated by a vertical laser sheet ($\lambda = 532\,\mathrm{nm}$) with a thickness of $200\,\mu$m, is imaged by an achromatic doublet on a CMOS sensor (Hamamatsu Orca-Flash 4.0, 2048×2048 square px. of side $6.5\,\mu$m) set at $\vartheta = 90°$ with respect to the illumination plane. Selection of a specific scattering wave-vector $q = (4\pi/\lambda)n\sin(\vartheta/2) \cong 1.15/R \approx 23\,\mu\mathrm{m}^{-1}$ is obtained by suitably stopping down the numerical aperture of the collection optics with a diaphragm placed in the focal plane of the imaging lens. The sample cell consists of a quartz cuvette with a width of 10 mm and a depth of 2 mm (Hellma, model 115F-QS). This cell geometry and the imaging optics allow us to laterally image a rectangular area S within the sample with a vertical extent $L \simeq 8.4\,\mathrm{mm}$ and a horizontal width $W \simeq 7\,\mathrm{mm}$, which allows mapping the sample region extending from the 1 mm from the right wall of the cell to about 2 mm from the left wall (see yellow region of Fig.1). The cell is partially filled with the sample in order to see the air-liquid meniscus and to measure the initial height h_0 of the gel. The cell is inserted into thermostatting holder, connected to a recirculating bath. During the whole duration of the experiment the temperature fluctuates less than 0.2° C. The hot water of the circulating bath enters in the cell holder from the top and exits from the bottom. This creates a vertical temperature gradient of less than 0.02° C/cm. We carefully checked for any slow sample evaporation by monitoring the position of the air-supernatant meniscus, which was found to be less than 1% in volume over the total duration of the experiment.

II. TIME EVOLUTION OF THE GEL AND SPATIO–TEMPORAL HETEROGENEITY

A. Gelation and gravity compression

The colloidal solution is initially poured at room temperature in the cuvette, and then quickly brought to the desired gelation temperature by inserting it into the (already thermalized) cell holder. With a delay of less than a couple of minutes required for the sample to reach the final temperature the sample starts to gel, as witnessed by a moderate increase of the scattered intensity and, as the same time, by a rapid slowing down of the speckle pattern dynamics. Conventionally, we define the gelation time t_g as the time at which the correlation index of two images taken at 1 s of delay (the minimum delay probed in our experiments) becomes larger than 0.1.

For $t > t_g$ the gel starts to compact smoothly under its own weight, with no macroscopic sign of gel rupture and with a compression kinetics that, as shown in the left panel of Figure 2, is highly non-linear in time. After a short initial quiescent state lasting for about 10^3 s, the gel displays two rather well separated restructuring stages, consisting of a first rapid collapse lasting for about 10^4 s followed by a much slower compaction. The inset of the left panel of Figure 2 shows that in the late compacting stage (for $t > 50000\,(s)$) the height $h(t)$ of the gel decreases exponentially, with a characteristic time of more than 3 days and an asymptotic limit amounting to a gel compression of about 20% [46].

A detailed analysis of the velocity profiles, obtained by monitoring with PCI the local displacements within the sample, confirms that the gel compression is fully ruled by gravity. The right panel of Figure 2 shows the (horizontally–averaged) velocity component along the vertical direction z for three values of the time t lapsed from sample preparation, ranging between $t = 2500\,\mathrm{s}$ (when the settling dynamics becomes slow enough to be reliably followed) and a maximum value of $t = 10^4\,\mathrm{s}$, after which the settling rate becomes so slow that the speckle pattern fully decorrelates because of the microscopic gel dynamics before it appreciably shifts downwards due to any residual sedimentation effect. Close to the cell bottom, where the structure is subjected to a gravitational stress larger than its yield stress, the settling speed increases with z, so the lower part of the gel consolidates. Conversely, on top of this region the velocity does not significatively depend on z, so the local volume fraction is basically fixed to its initial value and gel settles as a rigid body. Because we wish to focus on the gel restructuring after gravity compression has become negligible, in what follows we conventionally shift origin of the time axis to $t_0 = 12000\,\mathrm{s}$, when the system has fully entered the slow settling stage.

B. Speeding–up dynamics, the harbinger of macro–quakes

Several distinctive and rather surprising features of the gel restructuring dynamics are readily apparent from a qualitative description of the dependence on the aging time of temporal correlation over the *entire* gel. Namely, in this preliminary description we shall consider only averages of the correlation index over the whole investigated region of the gel, renouncing therefore to the spatial resolution provided by PCI to gain statistical accuracy. We shall indicate this space–averaged correlation index as $c_I(\tau; t)$, simply dropping the specification of the location

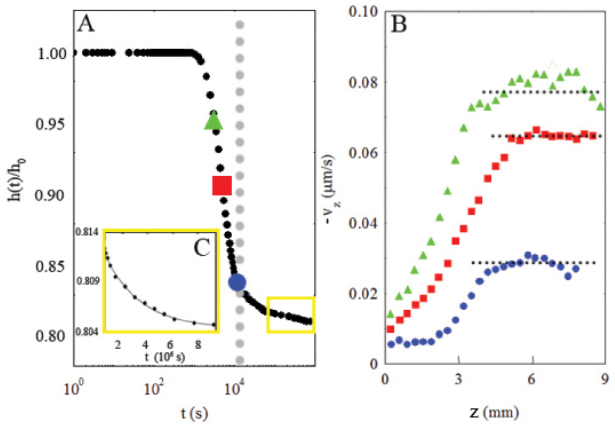

FIG. 2. Panel A: Decrease in time of the gel height $h(t)$ normalized to its initial value h_0. The dotted line marks the time $t = 12000$ when the gel enters the final slow stage of compression. Full symbols show the three values of t at which the velocity profiles in panel B are obtained. Panel B: Settling velocity profiles obtained $t = 2500, 5000, 10000$ s after gel preparation. Far enough from the cell bottom, the settling speed takes on approximately constant values, shown by the dotted lines. Panel C: Expanded view of the last stage of the compression stage (yellow box), with an exponential fit to the data for $h(t)$ (full line).

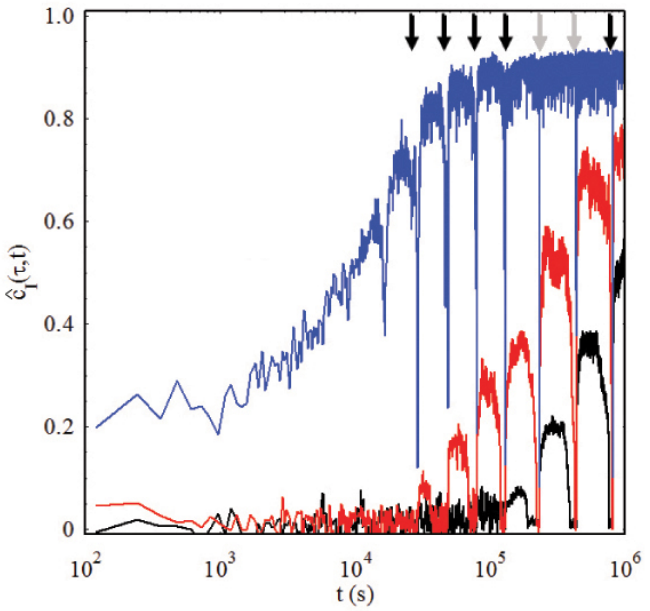

FIG. 3. Evolution of $\hat{c}_I(\tau;t)$ at delay times $\tau = 120\,\mathrm{s}$, $10800\,\mathrm{s}$ (3 h), and $43200\,\mathrm{s}$ (12 h), from top to bottom, over a timescale of about 12 days. The arrows mark the occurrence of 7 macro–quakes, conventionally identified by the times when, for the shortest delay, the normalized correlation coefficient drops below the value $\hat{c}_I = 0.5$. The two light arrows bound the interval of time between the 5^{th} and the 6^{th} MQ shown in Fig. 4 and extensively discussed in the text.

of the ROI it refers to. Besides, to describe the gel temporal dynamics we shall also introduce a *normalized* degree of correlation, defined as the ratio

$$\hat{c}_I(\tau;t) = \frac{c_I(\tau;t)}{c_I(0;t)}.$$

The dependence on the aging time t of this quantity, which may reasonably be expected to be less sensitive than c_I to the statistical fluctuation associated with the finite pixel sampling [47], is shown in Figure 3 for three values of the delay time τ.

Let us focus on the behavior of $\hat{c}_I(\tau;t)$ for the shortest delay time, $\tau = 120\,\mathrm{s}$, noticing first that $\hat{c}_I(120\,\mathrm{s};t)$ is finite and consistently larger than zero for all values of the aging time t. Since in the colloidal fluid region (for $T < T_{ps}$) the DLS correlation functions at the same q-vector fully decay in a few tens of milliseconds, this means that, once it has entered the slow settling stage, the system is already a quasi–arrested gel. For $t \gtrsim 10^5$ s, the correlation between the initial speckle pattern and a speckle pattern taken with a delay time $\tau = 120\,\mathrm{s}$ is almost complete, which means that, over the time scale of two minutes, the gel dynamics is basically arrested [48].

On top of this overall increasing trend, however, $\hat{c}_I(120\,\mathrm{s};t)$ displays a very 'spiky' behavior, characterized by two different kinds of sudden 'drops' in the normalized correlation index, associated with abrupt changes of the speckle pattern and arguably stemming from different types of rearrangement events within the gel. Indeed, a sequence of irregular minor drops, each one lowering $\hat{c}_I$ by less than the $10 - 15\%$, is intercalated by a few big decorrelation events, marked by the arrows in Figure 3, during which the correlation index plunges down to very low values. A qualitatively similar behavior is observed for the trend of $\hat{c}_I$ obtained at larger values of τ. Notably, the large decorrelation events very approximately occurs at the same time for all values of τ. We shall refer to one of these huge restructuring events as to a 'macro–quake' (MQ), whereas any smaller events will be dubbed a 'micro–quake' (μQ).

The gel dynamics fully unravels its very peculiar aging behavior if we focus on a time window between two consecutive MQs. In the panel A of Fig.4 we consider in detail the behavior of the correlation index $\hat{c}_I(\tau;t)$, shown for the same delays discussed in Figure 3, within the time interval between the 5^{th} and the 6^{th} large decorrelation events we detected, pinpointed by the two lighter arrows in Fig. 3. Because of the way it is constructed, $\hat{c}_I(\tau;\bar{t})$ at a given time $\bar{t}$ implicitly bears information about the subsequent behavior of the correlation index up to $\bar{t}+\tau$. Hence, if a full decorrelation event takes place in the time interval $\bar{t} \le t \le \bar{t}+\tau$, $\hat{c}_I(\tau;\bar{t})$ will drop to zero. In the panel A of Fig.4 the bullets on the t-axis show, for a fixed value of the delay τ, the time $t^*(\tau) = t_{MQ} - \tau$ when $\hat{c}_I(\tau;t)$ sharply drops due to the occurrence of the next MQ. In fact, for fixed τ the evolution of the correlation index with the gel age is meaningful only to the left of this points, since at $t = t^*(\tau)$ any memories of the fore-

going behavior is suddenly lost. Therefore, we can define for each MQ a sort of 'event horizon' as the straight line $\tau = t_{MQ} - t$ (shown for instance by the black line in panel B of Figure 4 for the 6$^{\text{th}}$ MQ). If we focus on the plot for the intermediate delay ($\tau = 3\,$h, red line), we can clearly set apart three distinct phases characterized by a markedly different dynamical behavior:

I) In the first phase, after a big rearrangement event has turned the whole gel into a dynamically active structure ($\hat{c}_I \simeq 0$), correlation is recovered on a time scale of a few hours, but the gel dynamics after recovery is much slower than before the MQ. We shall call this time interval the *recovery* phase;

II) The intermediate phase corresponds instead to a 'quiescent' state lasting for almost a day in which the gel dynamics is basically stationary. This quiet period will be dubbed the *slack* phase;

III) In the final phase, the microscopic dynamics unexpectedly starts to speed up and gets faster and faster for several hours until the successive MQ, marked by the red dot on the time axis (corresponding to the location of the 'event horizon' for $\tau = 3\,$h), takes place. This very interesting phase will be called the *jittery* phase.

A qualitatively similar behavior is found at longer delay ($\tau = 12\,$h, black line), while for the shortest delay ($\tau = 120\,$s, blue line) the dynamics between the two MQs is essentially stationary. The existence of this three phases can be better appreciated if we consider the curves $\tau(t)$ that give, as a function of t, the values of τ at which the correlation index takes on a fixed value. In the panel B of Fig.4 we show the two $\tau(t)$ curves corresponding to $c_I(\tau;t) = 0.3, 0.5$. The whole amount of information carried by $\hat{c_I}(\tau;t)$ can also be conveyed by the color map in the (τ,t) plane shown in Panel C of Fig. 4. For instance, note first that a horizontal cut of the map illustrates the time evolution of the correlation between the speckle patterns separated by a fixed delay $\bar{\tau}$ (like in the body of Figure 3 or in the panel A of Fig.4). If we plot some indicative contour lines we obtain the $\tau(t)$ curves shown in the panel B. Conversely the color–coded elevation profile of a vertical cut of the map yields the correlation index as a function of the delay τ for a fixed age $\bar{t}$ of the gel, which is fully equivalent to the intensity correlation function obtained in a standard DLS experiment. Looking at color map shown in the panel C of Fig.4, where the white dotted line indicates the 'event horizon' for the 6$^{\text{th}}$ MQ, it is clear how the huge decorrelation event is anticipated and heralded by a spontaneous speeding up of the microscopic dynamics. Such a progressive 'boost' of the local dynamics preceding an overall restructuring event is arguably the most notable finding of this investigation. As a matter of fact, this distinctive aging behavior is observed within all time windows between two successive MQs. Quantitatively, however, the slowing down of the dynamics gets more pronounced with the age of the gel. Indeed, when averaged over the slack time of each inter–quake period, the characteristic decay time of the microscopic dynamics, defined as the time-integral of the intensity correlation function, increases with aging time.

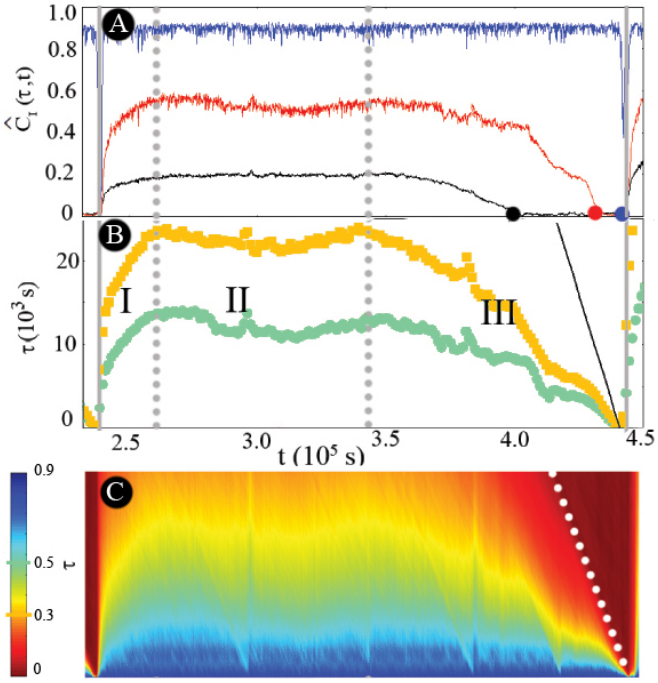

FIG. 4. Panel A: Time-evolution of $\hat{c}_I(\tau;t)$ at delay times $\tau = 120\,$s, 3 h, and 12 h (from top to bottom). The bullets on the t-axis show, for each value of τ, the time $t^*(\tau) = t_{MQ} - \tau$ when $\hat{c}_I(\tau;t)$ sharply drops due to the occurrence of the next MQ as described in the text. Panel B: Values of τ at which $\hat{c}_I(\tau;t)$ is equal to 0.5 (dots) or 0.3 (squares) versus the gel age t. The vertical gray lines show the limits of the interval bounded by the lighter arrows in Fig.3. The dashed lines separate the different aging regimes (the recovery, slack, and jittery phases) discussed in the text, while the black line $\tau = t_MQ - t$ is the 'event horizon'. Panel C: Color map of $\hat{c_I}(\tau;t)$ in the (τ,t) plane. The dotted line is the 'event horizon' discussed in the text.

C. From localized plastic events to global restructuring: the spreading of decorrelation bursts

So far, we have only investigated the dependence on gel aging of time correlations, averaged over the whole probed sample volume. PCI, however, also allows for a spatially–resolved investigation, which is crucial to single out where the restructuring events originate from, whether and how they propagate through the gel and, more generally, to what extent is the microscopic dynamics spatially heterogeneous.

Striking evidence of the spatial heterogeneity associated with a intermittent gel dynamics can be obtained by visualizing a single restructuring event using a so-called

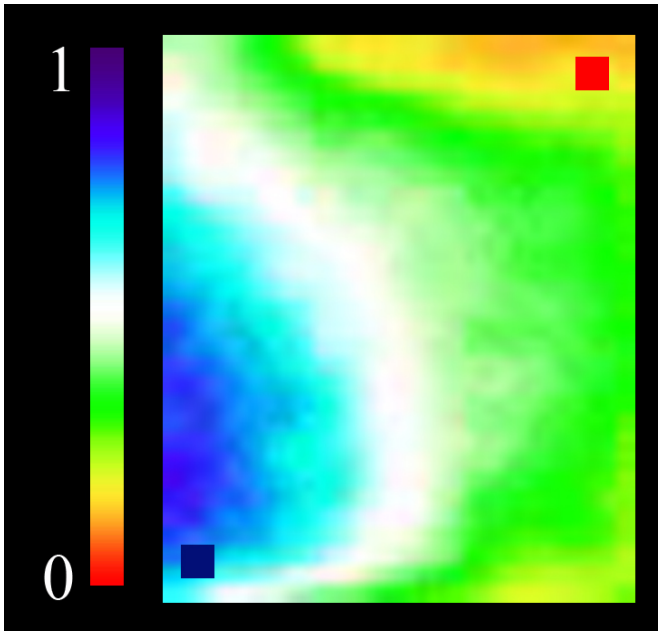

FIG. 5. Activity map averaged over the slack phase of the inter–quake period shown in Fig.4. The red (top-right) and blue (bottom-left) square regions highlighted in the first panel indicate, respectively, the 'fast' and 'slow' regions analyzed in details in the text. The scale displays the color scale for the normalized degree of correlation (field of view 7 mm×8.4 mm).

'dynamical activity map', where the spatial distribution of the correlation index is represented by a color map. To this aim, we have divided each sample image in 50×60 ROIs of size 20×20 pixels. Each of them is then attributed the average value of the normalized correlation index $\hat{c}_I(\tau; t, \mathbf{r})$ within the ROI, evaluated at given delay time τ. Fig. 5 shows the activity map $\langle \hat{c}_I(3\,\mathrm{h}; t, \mathbf{r})\rangle_{\mathrm{II}}$ obtained for $\tau = 3\,\mathrm{h}$ by averaging over the slack time (II) between two MQs (see Fig. 4). At this large value of the delay time τ, $\hat{c}_I(\tau; t, \mathbf{r}) > 0$ on every ROI, namely the whole sample is fully arrested. Yet, the map shows clear evidence of spatial heterogeneity: for instance, the region of the image at the upper right, which is close to the gel interface, clearly shows a restructuring dynamics faster than the region at the bottom left.

As further discussed in the following, such a time–averaged spatial heterogeneity map witnesses the propensity of all the gels we investigated to break more easily close to the meniscus separating them from the supernatant left above during the initial settling stage. We can get rid of this heterogeneity effect by introducing a 'normalized' activity map obtained by taking the ratio

$$\frac{\hat{c}_I(3\,\mathrm{h}; t, \mathbf{r})}{\langle \hat{c}_I(3\,\mathrm{h}; t, \mathbf{r})\rangle_{\mathrm{II}}}.$$

Fig. 6 shows a typical sequence of normalized maps referring to a *single* rearrangement event. While the map in frame (A) is obtained when the gel is still in the 'slack' phase (II), the maps from B to E show the progressive acceleration of the dynamics and its spreading through the whole gel in the 'jittery' phase (III). At a time approximately indicated by frame F a sudden and global rearrangement event (a MQ) occurs. Frames G to I illustrate the following 'recovery phase' (I). Notably, the last region that fluidizes is the first one where an arrested state is recovered. About 12 hours after this recovery phase has started, the whole gel has reverted to an arrested and quiescent state, and remains for a long time in this slack state until the whole process repeats (see also the video in SM).

Remarkably, all the MQs we observed in the gel originated from the top right of the sample [49]. To scrutinize whether this was just sheer coincidence or if some underlying physics favors this distinctive location, we have prepared several other gels using different cells or varying the heating protocol. Yet the point of origin of the MQ events, although varying among the samples, was invariably very close to the gel meniscus. This evidence suggests that the gravitational stress, which is of course stronger close to the cell bottom where the gel has to sustain its whole weight, is not the main cause of gel breaking.

We do not have a straightforward explanation of why these gels rearrange starting from the top. Yet, it is useful to point out that the initial compression stage unavoidably makes the gel spatially inhomogeneous and leads to nonnegligible vertical concentration gradients (in particular, the particle density close to the cell bottom is definitely larger than at the upper meniscus). The occurrence of inhomogeneity is confirmed by a spatial analysis of the gel dynamics. Indeed, let us compare the two ROIs indicated in Fig. 5 with a red and a blue square, corresponding to regions where the dynamics is, respectively, 'fast' and 'slow'. Figure 7 shows several (base–subtracted) correlations functions $g_2(\tau) - 1$ of these two regions at different aging times [50]. We see that, at the same aging time, the characteristic decay time of the correlation functions is one of magnitude shorted in the red region than in the blue one. In fact, in the blue region the dynamics is so slow that, when a novel MQ occurs, $g_2(\tau)$ is still significatively larger than one, hence it cannot be followed for longer delays (see the plots in top Panel in Figure 7). The correlation functions are approximately exponential in both the regions, although for what concern the 'fast' region, the exponential behaviour is limited only to the first four intervals between consecutive MQs in the 'fast' region. In fact, in the very late stage of gel aging ($t \gtrsim 2 \times 10^5\,\mathrm{s}$), the correlation functions in the 'fast' region start to display a complex and rather puzzling shape, which cannot anymore be fitted as an exponential–like decay.

It is instructive to consider the dependence of the relaxation time τ_r, both in the 'slow' and in the 'fast' region (for $t < 2 \times 10^5\,\mathrm{s}$), on the aging time t. The double–log plot Panel C in Fig. 7 shows that τ_r scales as a power law, $\tau_r \sim t^{\mu}$, with $\mu \simeq 1.17 \pm 0.05$. A similar 'hyper–aging' ($\mu > 1$) behaviour of the microscopic relaxation

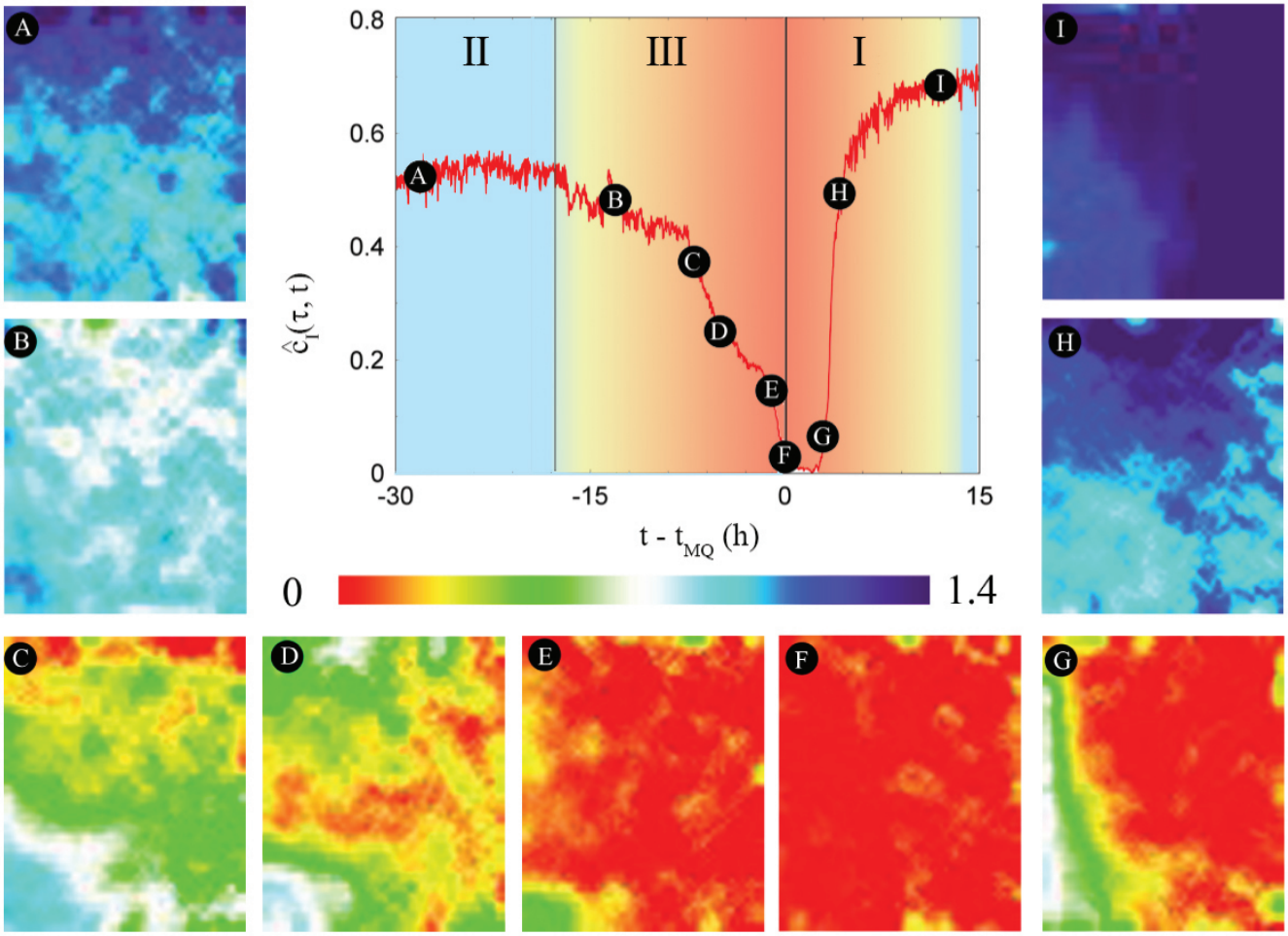

FIG. 6. Central Panel: Expanded view of the behavior of the normalized correlation index with approximate boundaries of the 'slack' (II), 'jittery' (III), and 'recovery' (I) phases, in a time region between -30 and +15 h around the 6^{th} MQ in Fig. 3 (taking place about 125 h after sample preparation). Letters within the black dots refer to the surrounding sequence of normalized activity maps, each one referring to a delay $\tau = 3$ h The values of the normalized correlation index $\frac{\hat{c}_I(3\,\mathrm{h};t,\mathbf{r})}{\langle \hat{c}_I(3\,\mathrm{h};t,\mathbf{r})\rangle_{\mathrm{II}}}$ are given by the color scale to the right (field of view 7 mm × 8.4 mm).

time has previously been observed in irreversible gels obtained by salt–induced colloidal aggregation [51]. What is most surprising, however, is that a very similar behavior is shared by the rate at which the large restructuring events take place. Panel C shows indeed that the waiting time δt_{MQ} between two consecutive MQs also behaves as a power law of the gel age, with a very similar exponent. This evidence strongly suggests a strong correlation between the progressive slowing down of the gel microscopic dynamics and the occurrence of system–spanning restructuring event. Note that $\mu > 1$ also implies that δt_{MQ} would eventually *exceed* the gel age: at this stage, no further MQs should in principle take place [52].

III. STATISTICS OF THE MICRO–QUAKES

As discussed in Section II B, during the slack time joining two MQ events the degree of correlation undergoes a large number of 'micro–quakes' qualitatively suggesting that, from time to time, sudden displacements of the local gel structure take place. To get a quantitative picture of these local rearrangements it is worth considering the probability density function (p.d.f.) of the values of the normalized correlation index [51, 53]. Since it takes values in the limited interval $[0, 1]$, however, $\hat{c}_I$ is rather inconvenient as a random variable. We rather found more useful to determine the p.d.f. of the quantity

$$\delta(\tau; t) = -q^{-1}(\ln(\hat{c}_I(\tau; t)))^{1/2}, \qquad (3)$$

which conversely, being defined for all $\delta > 0$, might hopefully follow one of the several types of distributions for

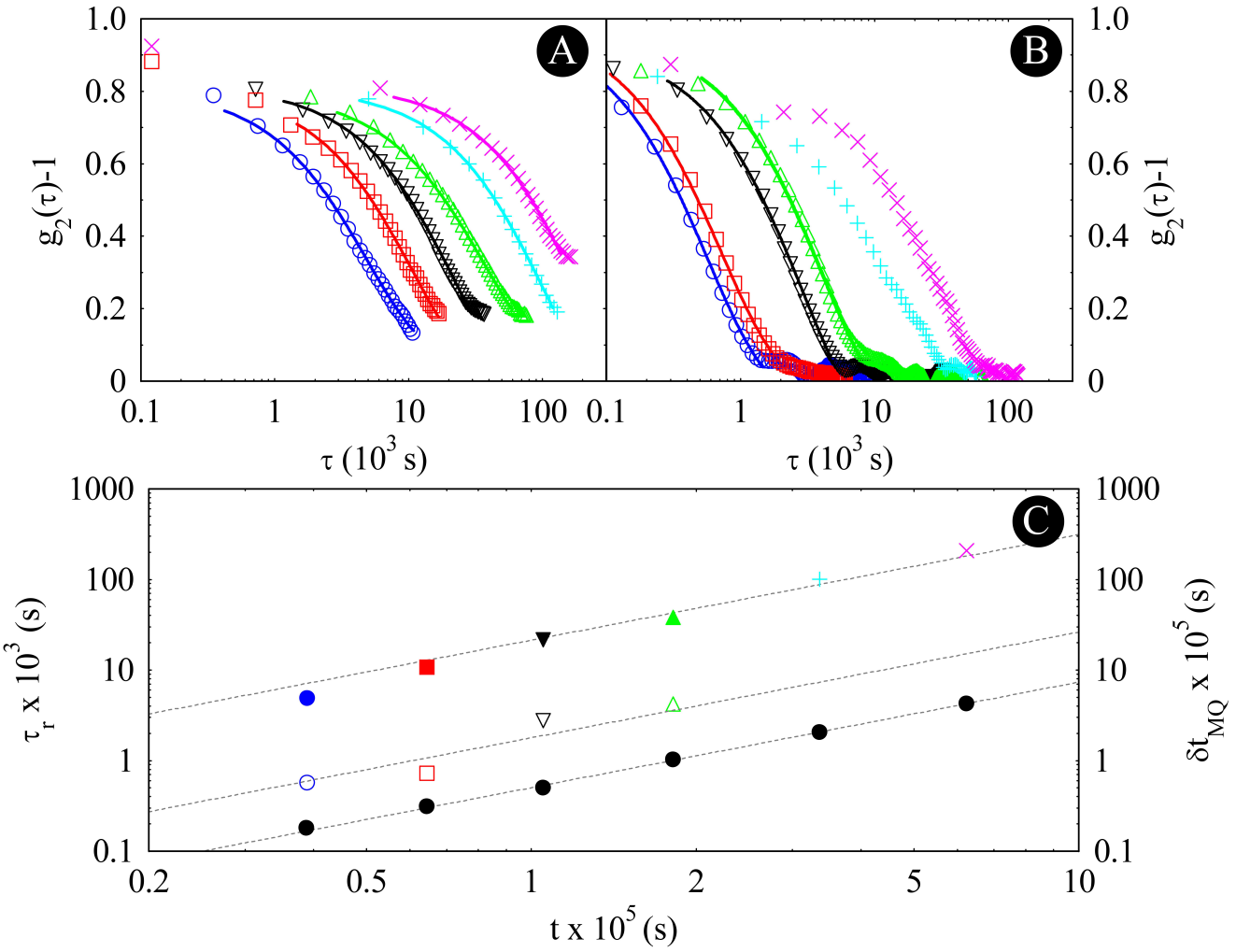

FIG. 7. Correlation functions $g_2(\tau) - 1$ in the 'slow' (Panel A) and in 'fast' (Panel B) regions defined in Fig. 5 fitted as simple exponentials as detailed in the text. Panel C: Values of the decay time τ_r plotted versus the aging time t using the same symbols as in the Panels above. Full and open symbols correspond to the 'slow' and 'fast' region respectively. Black dots are instead the values (right axis) of the waiting time between two consecutive MQs, while the three dashed lines are power laws with an exponent $\mu = 1.17$.

positive definite variables. For independent Brownian particles (or for a probe particle in a microrheology experiment), δ obviously coincides with the particle r.m.s. displacement $\langle \Delta r^2(t) \rangle^{1/2}$. In general this is not the case, but we can still loosely regard δ as an estimator of the average global rearrangement of the structure, gauged in units of the inverse of the scattering wave-vector q. In fact, like for an isolated particle free to diffuse, the scattered field would loose any correlation with its initial value after a time τ such that $\delta(\tau; t)q \sim \pi$. If we just consider those events happening within the slack time between two MQs, during which the dynamics is stationary, δ does not moreover explicitly depend on the aging time t.

Consider first the 'fast' region of the gel [54]. A detailed analysis of the fluctuations of the normalized correlation index, made for two values of delay time τ, yields the experimental p.d.f.'s for $\delta(\tau; t)$ displayed in the upper Panel of Fig. 8. At short delay ($\tau = 1$ min) the p.d.f. shows a pronounced tail to the right, namely a large positive skewness. The distribution becomes more symmetric by increasing τ to 30 min, but in both cases δ is far from being normally distributed, (which is what we would expect were the fluctuations due to a Brownian stochastic process). In particular, the semi–log plots show that the tails of the distribution are simple exponentials. This is often the hallmark of a logistic distribution, which is given in standard form by $p(z) = (1/4)\,\mathrm{sech}^2(z/2)$ and is basically the derivative of the Fermi function. Although a simple logistic is symmetric around its mean, it can be generalized to obtain a class of skewed p.d.f.'s. Among them, we found that, for all values of τ, the experimental

distributions for delta are nicely fitted by

$$p(\delta) = \frac{\sin(\pi\beta)}{\pi s(1-\beta)} \frac{\mathrm{e}^{-\beta(\delta-\delta_0)/s}}{\left[1+\mathrm{e}^{-(\delta-\delta_0)/s}\right]^2} \tag{4}$$

where β is a shape parameter taking values in the interval $[0, 2]$, and δ_0, s are simply related to the p.d.f. expectation $\langle\delta\rangle$ and variance σ^2 by

$$\begin{cases} \langle\delta\rangle = \delta_0 + s\left[\dfrac{1}{1-\beta} + \pi\cot(\pi\beta)\right] \\ \sigma^2 = s^2\left[\pi^2\csc^2(\pi\beta) - \dfrac{1}{(1-\beta)^2}\right] \end{cases} \tag{5}$$

This p.d.f. is actually a special case of a 'Generalized Logistic Distribution of type IV', whose properties are further discussed in the appendix A. The Inset of Figure 8 shows that, by increasing the delay time τ, the fitted values for β approach $\beta = 1$ from below: in this limit the p.d.f. becomes a simple logistic distribution.

In arrested systems, observing sequences of large structural rearrangements generating distributions of the fluctuations of a structural probe with non-Gaussian tails and a consistent skewness is anything but rare [51, 55–57]. Although no rigorous model leading to a specific statistics exists, in the case we are considering some general features of the p.d.f. for δ, and in particular its dependence on τ can be qualitatively grasped by considering a scenario where intermittent decorrelation events (the micro–quakes), taking place with an average frequency f, superimpose over faster and much weaker thermal fluctuations with a Gaussian distribution. Indeed, if τ is smaller or comparable to the average waiting time $1/f$, the probability of incurring into a micro–quake within a time window of width τ will be very small. Hence, the occurrence of these rare events should contribute to the p.d.f. as a tail towards large values of δ. Conversely, for $\tau \gg 1/f$, the p.d.f. will simply reflect the probability distribution for the amplitude of the micro–quakes, which may itself be a standard Gaussian (but not necessarily). To go beyond this very sketchy explanation, one should inquire about the origin of the sudden decorrelation events. As we already anticipated, these events should be attributed to the sudden release of local stresses frozen in the structure as a consequence of the rapid gelation process. In principle, for a deeply quenched and jammed material in which the thermal energy may nevertheless be comparable with the stored elastic energy, there are at least two mechanisms driving stress relaxation: spontaneous thermal fluctuations and elastic recovery of the structure[17]. These two mechanisms may in principle originate from two distinct populations of decorrelation events, which however are very difficult to set apart in the experimental frequency distributions for δ. Indeed, one may expect rearrangements of elastic origin to have a larger amplitude but, judging from the experimental p.d.f. we found, choosing a threshold for δ above which displacements should be attributed an elastic origin sounds rather arbitrary.

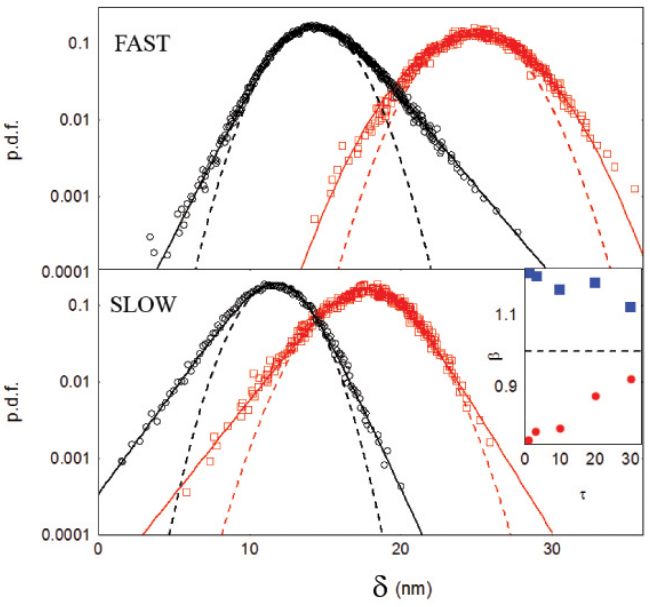

FIG. 8. Probability density functions for $\delta(\tau, t)$ in the fast (upper panel) and slow (lower panel) regions of the gel shown in Fig. 5, obtained for the delays $\tau = 1$ min (black circles) and $\tau = 30$ min (red squares). Continuous lines are the fit with the generalized logistic function defined in 4. The dashed line shows gaussian curves. Inset: Values of the β parameter in the fast (red dots) and slow (blue squares) for different delay times τ.

In order to characterize those large deviations from the mean associated with μQs of elastic origin, we found more useful to perform an Extreme Value Analysis (EVA), a strategy extensively used in disciplines, such as structural engineering, finance, earth sciences, traffic prediction, and geological engineering [58]. To this aim, we have split the sequence of values for δ in blocks of 100 samples (corresponding to a time duration of 100 min), extracting from each of them the maximum value δ_M.

Figure 9 shows that these maxima are distributed according to a Gumbel distribution,

$$G(\delta_M; m, s) = \frac{1}{s}\exp\left[\frac{\delta_M - m}{s} - \exp\left(\frac{\delta_M - m}{s}\right)\right], \tag{6}$$

where m, s are a location and a scale parameter related to the expectation and to the standard deviation by

$$\begin{cases} \langle\delta_M\rangle = m - \gamma s \\ \sigma(\delta_M) = (\pi/\sqrt{6})s \end{cases} \tag{7}$$

where $\gamma \simeq 0.577$ is the Euler–Mascheroni constant. The best fit to the data yields $\langle\delta_M\rangle \simeq 19$ nm and $\sigma(\delta_M) \simeq 3$ nm

According to a general result in EVA, the Fisher-Tippett-Gnedenko theorem [59–61], the Gumbel p.d.f. is one of the three classes of limiting distribution that can be obtained for the maxima of a sample of independent and identically distributed random variables [62]. No-

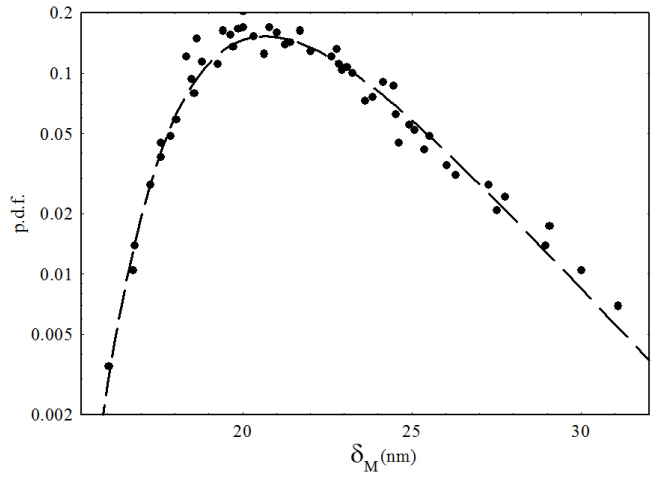

FIG. 9. p.d.f. of the maxima of δ within 100 min time slots fitted with a the Gumbel distribution with parameters $m = 20.7$ nm and $s = 2.4$ s.

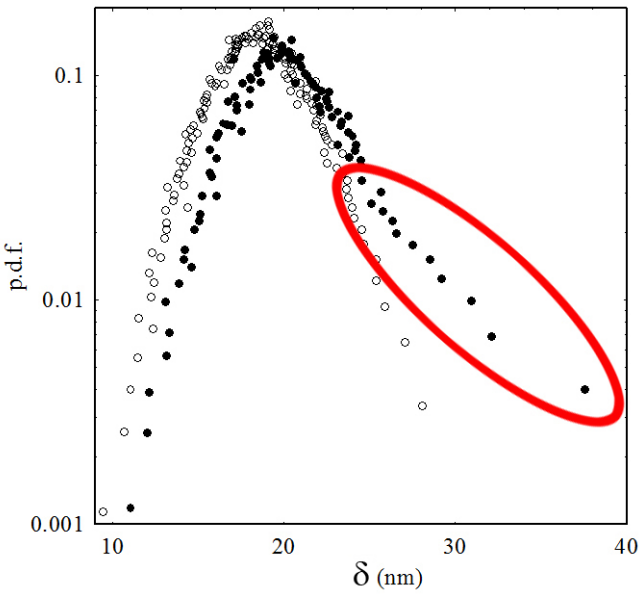

FIG. 10. Experimental distributions of $\delta(\tau, t)$ obtained for a delay time $\tau = 10$ min, in the slack (open circles) and in the jittery (full dots) phases respectively. The occurrence of long–time tail in the latter is highlighted in red.

tably, the logistic distribution belongs, together with several common distributions like the Gamma and the log–normal, to the 'domain of attraction' of the Gumbel distribution, namely to the class of distribution whose sampled maxima converge to $G(\delta_M; m, s)$ [61]. Even more interestingly, having found a Gumbel distribution for the maxima basically excludes that the p.d.f for δ decays very slowly, for instance as a power law.

The activity maps in Figure 6 show however that during the subsequent jittery phase, when the dynamics of the system gets faster, the spatial correlations between different ROIs becomes much more long–ranged, suggesting that the energy released by a localized event may trigger an avalanche of restructuring events spanning a large fraction of the gel. In this regime the probability of observing large drops of the correlation index significatively increases, which will arguably affect the p.d.f. for δ. To check for this additional contribution, in Fig. 10 we contrast the p.d.f.'s for $\delta(\tau; t)$ obtained with a delay $\tau = 10$ min in the slack (open circles) and in the jittery phase (full dots) [63]. The latter shows indeed a high–value tail which decays slower and with a marked change of slope.

Further information can be gained by considering the behavior of $\delta(\tau; t)$ in the slow region. The lower panel of Fig. 8 shows that, for this region too, the experimental distributions of $\delta(\tau; t)$ for two different delay times are not Gaussian either and can still be fitted using the generalized logistic distribution defined in Eq. 4. Yet, at variance with what we found for the fast region, the p.d.f. is markedly skewed towards *smaller* values of δ. Once again, a longer delay time yields a more symmetric distribution. However, the inset in Fig. 8 shows that, by increasing the delay time, the β parameter approaches unity from *above*. At the moment we do not have a straightforward explanation of this peculiar behaviour. Therefore, although their general behavior is similar, the statistical distribution for the slow and fast regions display some relevant and rather puzzling differences, mostly concerning their asymmetry and the dependence of the latter on the delay time.

To further inquire about these differences, it is particularly useful to consider a detailed map of the asymmetry of the statistical distribution of the values of δ over the different regions of the gel, which is directly related to the value of the β parameter, with $\beta = 1$ corresponding to zero skewness. To increase the statistical accuracy, we grouped together adjacent ROIs, generating a map of 7×8 'macro-ROIs'. We evaluated the experimental distribution of δ in the slack phase on each of these enlarged ROI for a delay $\tau = 1$ min, and fitted them using a modified logistic distribution. The 'asymmetry' map we obtained is shown in Panel A of Fig. 11. Notably, the spatial distribution of β turns out to be strongly correlated with the local dynamics of the sample encoded in the activity maps shown in Fig. 6 (see for instance Panel C). The occurrence of a consistent degree of correlation can be visually appreciated by contrasting Panel A with Panel B, where a lower resolution version of frame C in Fig. 7, obtained by averaging the values of the normalized correlation index $\hat{c}_I(3\,\mathrm{h}; t, \mathbf{r}) / \langle \hat{c}_I(3\,\mathrm{h}; t, \mathbf{r}) \rangle_{\mathrm{II}}$ between adjacent ROIs so to obtain an activity map with the same number of pixels as the 'asymmetry' map. It is important to stress that the p.d.f. is extracted by images taken at the short delay time $\tau = 1$ min, while the typical restructuring time of the gel is of the order of $10^3 - 10^5$ s. Our result open the possibility to predict the long time restructuring dynamics of a gel analyzing the statistics of its short time rearrangement events. We are currently

investigating if this result is general and holds also for different kinds of physical gels.

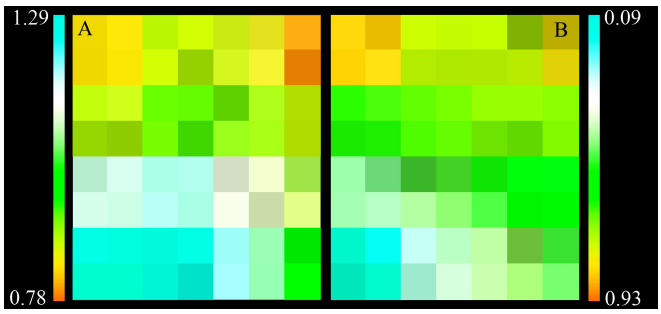

FIG. 11. Panel A: 'Asymmetry' map calculated as described in the text. The values of the β parameter of the generalized logistic distribution are given by the color scale at the left. Panel B: Normalized activity map at the same aging time of the frame C in Fig. 6, with the values for the normalized correlation index $(\hat{c}_I(3\,\mathrm{h}; t, \mathbf{r})/\langle \hat{c}_I(3\,\mathrm{h}; \mathbf{r})\rangle$ given by the color scale at the right.

IV. DISCUSSION

The investigation we performed shows that the aging of physical colloidal gels is arguably far richer than previously conceived. Among the evidence we presented, it is worth emphasizing the concurrence of spatially–localized 'micro-quakes' with system–spanning 'macro-quakes', the observation of a speeding up of the microscopic dynamics acting as 'harbinger' of a MQ, and the distinctive dependence of the waiting time between two MQs on the age of the gel. In this closing remarks, we suggest that a qualitative explanation of these peculiar effects may be grounded on the spontaneous occurrence of slow viscoelastic modes in highly porous materials.

Let us first focus on the occurrence of distinct scales of magnitude and occurrence rate for the restructuring events. While this seems to be a novel feature of the spontaneous aging of soft materials, in driven systems such as structures subjected to a progressive accumulation of load the concurrence of localized restructuring processes with system–spanning rearrangements is by no means unusual. For instance, whereas the seismic moment (or the amount of released energy) of the earthquakes generated by a fault *system* is generally distributed according to the scale–free Gutenberg–Richter law, on a *single* fault large earthquakes often occur with a typical magnitude much larger than what could be expected extrapolating from the distribution of the weak seismic events, and often occur at a rather constant rate [38, 39]. This quasi–periodic occurrence of large upheavals in specific geographical areas is a manifestation of the so-called 'seismic cycle'. It is nevertheless important to stress a relevant difference between seismic and gel quakes. Earthquakes are usually associated with macroscopic ruptures in a fault. Conversely the MQs we are considering amount to a full 'fluidization' of the gel structure on the small spatial scale of a few particles, while on macroscopic scales the gel still behaves as a solid. Similarly, the response of micro–crystals to a slow but continuous compression has recently been found to consist of periods of stress accumulation followed by sudden bursts of released energy ('avalanches') leading to irreversible reorganization at the micro–scale [28]. This evidence can be accounted for by assuming that the relaxation of internal stresses derives from the concurrence of a dominant elasto–plastic (EP) mechanism, which accounts for the occurrence of sudden huge restructuring events ('avalanches'), with additional dissipative effects acting during the quiescent periods between two avalanches. The nature of these secondary stress–relief mechanisms, which are neglected in standard EP models, may be the most varied, ranging from viscous dissipation in aquifers, dislocation flow in crystals, viscoelastic relaxations in soft materials. The synergy between these two sources of stress relaxation is captured by the concept of 'self-organized avalanche oscillator', which also provides a rationale for the quasi–periodicity of the large restructuring events [28].

This general concept is very well exemplified by a simple but powerful model where the secondary stress–dissipation effects are incorporated with the explicit strategy of generating earthquakes patterns similar to those observed in seismic phenomena [64, 65], which in spite of its simplicity generates the concurrence of small avalanches with periodic system–spanning quakes. With this approach, the material is still regarded as a made of mesoscopic blocks like in the EP model [19], but the latter interact like in a Standard Linear Solid, whose constitutive model is represented by a spring in parallel with the series combination of a spring and a dashpot. In this model big events are therefore anticipated by an increase of the frequency and amplitude of the μQs, a key feature shared by a recently proposed model that aims to spot the origin of seismic cycles by using the well-established concept of 'epidemic-type sequence' for the occurrence aftershocks [39]. In this model, any earthquakes can trigger new quakes. The key parameter of the process is the average number of 'daughter' earthquakes, n, which grows with the strength of the 'mother' event. For $n < 1$ the seismicity is characterized by a single family of earthquakes and there is not evidence of an increase of the earthquake rate approaching a big event: in the jargon of out-of-equilibrium phase transitions characterized by scale-free behaviour, the system is 'subcritical'. When $n > 1$, however, the system becomes 'supercritical' and enters a nonlinear regime: the stronger is the maximum sampled earthquake, the more copious is the cascade of daughter events. This self-reinforcing mechanism leads to an increase of the number earthquakes while the instant of a main-shock is approached. The case $n > 1$, for instance, characterizes the seismic activity anticipating the earthquake with magnitude $M = 6.8$ that occurred in 1984 in Nagano Prefecture, Japan [39, 66].

A speeding up of the dynamics heralding catastrophic

events has clearly been observed in a recent investigation where, by applying a constant shear stress and using an original setup that combines scattering and rheology, the macroscopic deformation and microscopic dynamics of colloidal gels were simultaneously measured [67]. During the first stage of the deformation the gel was found to behave elastically, which a negligible plastic yield. When the strain becomes sufficiently large the plastic activity becomes stronger, anticipating the failure of the material.

Several features of the models we have sketched could not be solely shown by driven systems, but also by systems displaying spontaneous restructuring processes in the absence of a driving force. In soft colloidal gels, for instance, distinctive viscoelastic stress–relaxation mechanisms are naturally present [68], stemming for instance from the slower motion of the solvent through the solid network as a consequence of a microscopic rupture event. We regard these slow viscoelastic dissipation modes, supported by random thermal agitation (which is not taken into account in purely mechanical models) as the most probable microscopic origin for the striking affinity between many of the features we observed in the spontaneous aging of gels and the predictions of the models for driven systems we mentioned. These similarities include the existence of a 'slack' phase characterized by a stationary dynamics and by the occurrence of localized and independent μQs; the subsequent onset of a 'jittery' phase when the microscopic dynamics accelerates and larger μQs with a different statistics becomes more probable, a dynamical stage that is the distinctive harbinger of a global restructuring event, after which system slowly recovers a new arrested state. Some discrepancy with the model prediction however exist. Indeed, while for a system driven by a constant load these models predict quasi–periodic global restructuring events, the separation between subsequent MQs grows with the gel age and is almost linearly related to the slowing–down of the microscopic dynamics. Notably, an increase of the characteristic relaxation time with sample age is compatible with the theoretical predictions of a model based on stress–dipole relaxation [69]. In this model, localized micro-collapses induce a tensile strain on the surrounding regions that increases the energy barrier for rearrangement and make the occurrence of a quake less probable. This 'hardening' mechanism yields a rate of the events that increases linearly in time. Although our findings suggest that stress relaxation in colloidal gel is more complex that assumed in [69], we point out that the rate of the μQs decreases from a slack phase to the next one. If the reduction of the avalanche frequency after each MQ follows the kinetics proposed in [69], a quasi-linear increase of δt_{MQ} with the sample age naturally emerges. To check if the gel actually hardens while aging, it would be useful measuring the mechanical properties of the gel after each MQ, for instance to check whether the elastic modulus grows with time as observed for biopolymer gels [7].

One may finally wonder whether the ageing processes we observed are truly spontaneous, or if the tiny gravity compression effects that still persist in the gel all along the aging period act as a crucial driving force. However, if the structural reorganization of the sample is induced by the very small strain rate of the settling gel, the microscopic restructuring time τ_r of the system should scale with the inverse of the strain rate [8, 37, 70], which we found to decay exponentially with time (see inset C of Fig. 2). Conversely, the results shown in Fig. 7 indicate that the microscopic restructuring time of the sample scales quasi-linearly with the aging time, suggesting that gravity should not play a leading role in setting the quake dynamics. We rather believe that this role is to be attributed to the stresses generated over large spatial regions of the gel during both the network formation and its initial compression. Assuming that the restructuring process is eventually driven by strong frozen-in elastic stresses is supported by the evidence of strong dynamic heterogeneity we detected and by the observation that the acceleration of the dynamics unavoidably originates from the same region of the gel. With regard to this specific issue, it is useful to point out that 2D simulations of the EP model with viscoelastic relaxation evidence a strong spatial correlation between the location of the origin of a MQ and that of the following quakes [64], with the MQ taking place within the most stressed region of the sample and the stress being released through aftershocks that diffuse away from the originating quake. However, what may be the origin of such a macroscopic stress heterogeneity in our samples is still an open question. A possible residual contribution of the gravitational stress is not fully ruled out. To settle this question, we have planned a series of microgravity measurements to be performed in the framework of the Project 'Colloid Solidification in Space' of the European Space Agency. Preliminary tests are currently being performed on the Light Microscopy Module on board of the International Space Station in the context of the NASA 'ACE-T10' mission.

ACKNOWLEDGMENTS

We acknowledge funding from the Italian Ministry for Education, University and Research (PRIN Project ID 2017Z55KCW - 'Soft Adaptive Networks') and thank U.C. Palmiero for particle synthesis, A. Mollame for preliminary characterization of the gels dynamics at different temperatures, and L. Cipelletti for useful discussions.

Appendix A: Generalized Logistic Distribution

In this appendix we report some useful mathematical properties of the *Generalized Logistic Distribution of type IV (GLD-IV)*. The introduction in literature of the GLD-IV is motivated by the need to generate a general three- or four-parameter family of distributions on the real line from the (two-parameter) logistic distribution as a start-

ing point. The two parameters of the logistic distribution are location x_0 and scale σ) The extra, shape, parameters should accommodate skewness and different amounts of tail-weight/kurtosis in some appropriate way, and hence afford more flexible and more robust modelling of data. The idea of Jones for the generation of such a family from the starting point of an arbitrary symmetric distribution is to utilize the set of its order statistic distributions (see [71] for an exhaustive mathematical discussion). The canonical ($x_0 = 0$ and $\sigma = 1$) GLD-IV is the probability distribution with density:

$$f_{\alpha,\beta}(x) = \frac{1}{B\left(\alpha,\beta\right)} \frac{e^{-\beta x}}{\left(1+e^{-x}\right)^{\alpha+\beta}} \tag{A1}$$

where B is the beta function defined as

$$B(x,y) = \int_0^1 t^{x-1}(1-t)^{y-1}dt = \frac{\Gamma(x)\Gamma(y)}{\Gamma(x+y)}. \tag{A2}$$

A general GLD-IV can be easily be obtained using the simple transformation $x \to \frac{x-x_0}{\sigma}$. While formally a GLD-IV depends on four parameter, one among σ, α, β is redundant in practice, because two parameters are actually sufficient to accommodate scale as well as skewness [72]. While usually the scale σ is fixed to 1, we found more useful to impose $\alpha = 2 - \beta$, obtaining:

$$\begin{aligned} B(2-\beta,\beta) = \Gamma(2-\beta)\Gamma(\beta) = \\ = (1-\beta)\Gamma(1-\beta)\Gamma(\beta) = \frac{\pi(1-\beta)}{\sin\left(\pi\beta\right)}, \end{aligned} \tag{A3}$$

where we use the Euler reflection formula. The density of the GLD-IV simplifies as:

$$f_2(x) = \frac{\sin(\pi\beta)}{\pi(1-\beta)} \frac{e^{-\beta x}}{(1-e^{-\alpha x})^2}. \tag{A4}$$

Exploiting the Eulero reflection formula is it possible to calculate the moment-generating function

$$M_x(t) = \frac{\Gamma(\beta-t)\Gamma(\alpha+t)}{\Gamma(\alpha)\Gamma(\beta)} \tag{A5}$$

with $(-\alpha < t < \beta)$.
For $\alpha + \beta = 2$ we have

$$\Gamma(\beta-t)\Gamma(2-(\beta-t)) = \frac{(1-\beta+t)\pi}{\sin(\pi(\beta-t))} \tag{A6}$$

and

$$\Gamma(\beta)\Gamma(2-\beta) = \frac{\pi(1-\beta)}{\sin\left(\pi\beta\right)} \tag{A7}$$

which give

$$M = \frac{(1-\beta+t)}{(1-\beta)} \frac{\sin\left(\pi\beta\right)}{\sin\left(\pi(\beta-t)\right)} \tag{A8}$$

For the general distribution function with $x \to \frac{x-x_0}{\sigma}$ the GLD-IV is

$$f_2(x) = \frac{\sin\left(\pi\beta\right)}{\pi\sigma(1-\beta)} \frac{e^{-\beta(x-x_0)/\sigma}}{\left(1+e^{-(x-x_0)/\sigma}\right)^2} \tag{A9}$$

The associated momenta are:
Expectation

$$\langle x \rangle = \sigma\left(\frac{1}{1-\beta} + \pi\cot\left(\pi\beta\right)\right) + x_0 \tag{A10}$$

Variance

$$\sigma_x^2 = \sigma^2\left(\frac{\pi^2}{(\sin\left(\pi\beta\right))^2} - \frac{1}{(1-\beta)^2}\right) \tag{A11}$$

Skew

$$\begin{aligned} \gamma = \frac{2\sigma^3\left(\pi^3\cot(\pi\beta)\mathrm{cosec}^2(\pi\beta) + \frac{1}{(1-\beta)^3}\right)}{\sigma^3\left(\pi^2\mathrm{cosec}^2(\pi\beta) - \frac{1}{(1-\beta)^2}\right)^{\frac{3}{2}}} = \\ = \frac{2}{\sigma_x}\left[\left(\langle x\rangle - x_0\right)\left(1 + \frac{\sigma^2}{\sigma_x^2(1-\beta)^2} - \frac{\sigma}{1-\beta}\right)\right] \end{aligned} \tag{A12}$$

The maximum of the distribution it is located at

$$x_{max} = x_0 + \sigma\ln\left(\frac{2-\beta}{\beta}\right) \tag{A13}$$

and its value is

$$f_2(x_{max}) = \frac{\sin(\pi\beta)}{\pi\sigma(1-\beta)}\left(\frac{\beta}{2-\beta}\right)^{\beta}\left(\frac{2-\beta}{2}\right)^2. \tag{A14}$$

The expansion of the $f_2(x)$ as a gaussian distribution around the x_{max} gives

$$\begin{aligned} f_{Gauss}(x) = \frac{\sin(\pi\beta)}{\pi\sigma(1-\beta)}\left(\frac{\beta}{1-\beta}\right)^{\beta}\left(\frac{2-\beta}{2}\right)^2 \\ \times\exp\left[-\frac{\left(x-x_{max}\right)^2}{2\left(\frac{2\sigma^2}{\beta(2-\beta)}\right)}\right]. \end{aligned} \tag{A15}$$

[1] L. Cipelletti, S. Manley, R. C. Ball, and D. A. Weitz, *Universal aging features in the restructuring of fractal colloidal gels*, Phys. Rev. Lett. **84**, 2275 (2000).

[2] E. Zaccarelli, *Colloidal gels: equilibrium and non–equilibrium routes*, J. Phys.: Condens. Matter **19**, 323101 (2007).

[3] P. I. Hurtado, L. Berthier, and W. Kob, *Heterogeneous diffusion in a reversible gel*, Phys. Rev. Lett. **98**, 135503 (2007).

[4] P. Chaudhuri, L. Berthier, P. I. Hurtado, and W. Kob, *When gel and glass meet: A mechanism for multistep relaxation*, Phys. Rev. E **81**, 040502 (2010).

[5] E. Del Gado, A. Fierro, L. de Arcangelis, and A. Coniglio, *Slow dynamics in gelation phenomena: From chemical gels to colloidal glasses*, Phys. Rev. E **69**, 051103 (2004).

[6] S. Buzzaccaro, R. Rusconi, and R. Piazza, *"Sticky" hard spheres: Equation of state, phase diagram, and metastable gels*, Phys. Rev. Lett. **99**, 098301 (2007).

[7] E. Secchi, T. Roversi, S. Buzzaccaro, L. Piazza, and R. Piazza, *Biopolymer gels with "physical" cross-links: Gelation kinetics, aging, heterogeneous dynamics, and macroscopic mechanical properties*, Soft Matter **9**, 3931 (2013).

[8] E. Secchi, S. Buzzaccaro, and R. Piazza, *Time-evolution scenarios for short-range depletion gels subjected to the gravitational stress*, Soft Matter **10**, 5296 (2014).

[9] E. Secchi, F. Munarin, M. Alaimo, S. Bosisio, S. Buzzaccaro, G. Ciccarella, V. Vergaro, P. Petrini, and R. Piazza, *External and internal gelation of pectin solutions: Microscopic dynamics versus macroscopic rheology*, J. Phys.: Condens. Matter **26**, 464106 (2014).

[10] D. Calzolari, I. Bischofberger, F. Nazzani, and V. Trappe, *Interplay of coarsening, aging, and stress hardening impacting the creep behavior of a colloidal gel*, J. Rheol. **61**, 817 (2017).

[11] O. Lieleg, J. Kayser, G. Brambilla, L. Cipelletti, and A. Bausch, *Slow dynamics and internal stress relaxation in bundled cytoskeletal networks*, Nat. Mater. **10**, 236 (2011).

[12] C. Perge, N. Taberlet, T. Gibaud, and S. Manneville, *Time dependence in large amplitude oscillatory shear: A rheo-ultrasonic study of fatigue dynamics in a colloidal gel*, J. Rheol. **58**, 1331 (2014).

[13] J. Conrad, H. Wyss, V. Trappe, S. Manley, K. Miyazaki, L. Kaufman, A. Schofield, D. R. Reichman, and D. Weitz, *Arrested fluid-fluid phase separation in depletion systems: Implications of the characteristic length on gel formation and rheology*, J. Rheol. **54**, 421 (2010).

[14] J. Colombo and E. Del Gado, *Stress localization, stiffening, and yielding in a model colloidal gel*, J. Rheol. **58**, 1089 (2014).

[15] P. J. Lu, E. Zaccarelli, F. Ciulla, A. B. Schofield, F. Sciortino, and D. A. Weitz, *Gelation of particles with short-range attraction*, Nature **453**, 499 (2008).

[16] F. Cardinaux, T. Gibaud, A. Stradner, and P. Schurtenberger, *Interplay between spinodal decomposition and glass formation in proteins exhibiting short-range attractions*, Phys. Rev. Lett. **99**, 118301 (2007).

[17] M. Bouzid, J. Colombo, L. V. Barbosa, and E. Del Gado, *Elastically driven intermittent microscopic dynamics in soft solids*, Nat. Commun. **8**, 15846 (2017).

[18] P. Chaudhuri and L. Berthier, *Ultra-long-range dynamic correlations in a microscopic model for aging gels*, Phys. Rev. E **95**, 060601 (2017).

[19] A. Nicolas, E. E. Ferrero, K. Martens, and J.-L. Barrat, *Deformation and flow of amorphous solids: Insights from elastoplastic models*, Rev. Mod. Phys. **90**, 045006 (2018).

[20] J. Lauridsen, M. Twardos, and M. Dennin, *Shear-induced stress relaxation in a two-dimensional wet foam*, Phys. Rev. Lett. **89**, 098303 (2002).

[21] D. M. Robe, S. Boettcher, P. Sibani, and P. Yunker, *Record dynamics: Direct experimental evidence from jammed colloids*, EPL **116**, 38003 (2016).

[22] S. Buzzaccaro, M. D. Alaimo, E. Secchi, and R. Piazza, *Spatially: resolved heterogeneous dynamics in a strong colloidal gel*, J. Phys.: Condens. Matter **27**, 194120 (2015).

[23] B. W. Mansel and M. A. Williams, *Internal stress drives slow glassy dynamics and quake-like behaviour in ionotropic pectin gels*, Soft Matter **11**, 7016 (2015).

[24] D. V. Denisov, K. A. Lőrincz, W. J. Wright, T. C. Hufnagel, A. Nawano, X. Gu, J. T. Uhl, K. A. Dahmen, and P. Schall, *Universal slip dynamics in metallic glasses and granular matter–linking frictional weakening with inertial effects*, Sci. Rep. **7**, 43376 (2017).

[25] J. Baró, Á. Corral, X. Illa, A. Planes, E. K. Salje, W. Schranz, D. E. Soto-Parra, and E. Vives, *Statistical similarity between the compression of a porous material and earthquakes*, Phys. Rev. Lett. **110**, 088702 (2013).

[26] T. Mäkinen, A. Miksic, M. Ovaska, and M. J. Alava, *Avalanches in wood compression*, Phys. Rev. Lett. **115**, 055501 (2015).

[27] J. Rosti, J. Koivisto, L. Laurson, and M. J. Alava, *Fluctuations and scaling in creep deformation*, Phys. Rev. Lett. **105**, 100601 (2010).

[28] S. Papanikolaou, D. M. Dimiduk, W. Choi, J. P. Sethna, M. D. Uchic, C. F. Woodward, and S. Zapperi, *Quasi-periodic events in crystal plasticity and the self-organized avalanche oscillator*, Nature **490**, 517 (2012).

[29] B. Ruta, Y. Chushkin, G. Monaco, L. Cipelletti, E. Pineda, P. Bruna, V. M. Giordano, and M. Gonzalez-Silveira, *Atomic-scale relaxation dynamics and aging in a metallic glass probed by x-ray photon correlation spectroscopy*, Phys. Rev. Lett. **109**, 165701 (2012).

[30] Z. Evenson, B. Ruta, S. Hechler, M. Stolpe, E. Pineda, I. Gallino, and R. Busch, *X-ray photon correlation spectroscopy reveals intermittent aging dynamics in a metallic glass*, Phys. Rev. Lett. **115**, 175701 (2015).

[31] K. A. Dahmen, Y. Ben-Zion, and J. T. Uhl, *Micromechanical model for deformation in solids with universal predictions for stress-strain curves and slip avalanches*, Phys. Rev. Lett. **102**, 175501 (2009).

[32] J. Bouchaud and A. Georges, *Anomalous diffusion in disordered media: Statistical mechanisms, models and physical applications*, Phys. Rep. **195**, 127 (1990).

[33] L. Berthier, G. Biroli, J.-P. Bouchaud, L. Cipelletti, and W. van Saarloos, *Dynamical heterogeneities in glasses, colloids, and granular media*, Vol. 150 (OUP Oxford, 2011).

[34] R. Piazza, Optical correlation techniques for the investigation of colloidal systems, in *Colloidal Foundations of Nanoscience*, edited by Elsevier (Elsevier, Amsterdam,

2004) Chap. 8.
[35] A. Duri, D. Sessoms, V. Trappe, and L. Cipelletti, *Resolving long-range spatial correlations in jammed colloidal systems using photon correlation imaging*, Phys. Rev. Lett. **102**, 085702 (2009).
[36] L. Cipelletti, G. Brambilla, S. Maccarrone, and S. Caroff, *Simultaneous measurement of the microscopic dynamics and the mesoscopic displacement field in soft systems by speckle imaging*, Opt. Express **21**, 22353 (2013).
[37] G. Brambilla, S. Buzzaccaro, R. Piazza, L. Berthier, and L. Cipelletti, *Highly nonlinear dynamics in a slowly sedimenting colloidal gel*, Phys. Rev. Lett. **106**, 118302 (2011).
[38] D. Bowman, G. Ouillon, C. Sammis, A. Sornette, and D. Sornette, *An observational test of the critical earthquake concept*, J. Geophys. Res.: Solid Earth **103**, 24359 (1998).
[39] D. Sornette and A. Helmstetter, *Occurrence of finite-time singularities in epidemic models of rupture, earthquakes, and starquakes*, Phys. Rev. Lett. **89**, 158501 (2002).
[40] V. Degiorgio, R. Piazza, and T. Bellini, *Static and dynamic light scattering study of fluorinated polymer colloids with a crystalline internal structure*, Adv. Colloid Interface Sci. **48**, 61 (1994).
[41] U. C. Palmiero, A. Agostini, E. Lattuada, S. Gatti, J. Singh, C. T. Canova, S. Buzzaccaro, and D. Moscatelli, *Use of raft macro–surfmers for the synthesis of transparent aqueous colloids with tunable interactions*, Soft Matter **13**, 6439 (2017).
[42] T. Staudt, M. C. Lang, R. Medda, J. Engelhardt, and S. W. Hell, *2,2 '-thiodiethanol: A new water soluble mounting medium for high resolution optical microscopy*, Microsc. Res. Tech. **70**, 1 (2007).
[43] J. Ulama, M. Z. Oskolkova, and J. Bergenholtz, *Monodisperse pegylated spheres: An aqueous colloidal model system*, J. Phys. Chem. B **118**, 2582 (2014).
[44] Equivalently, within the standard mapping of a colloidal suspension onto an effective one–component fluid, this is what is expected for a system of particles interacting via very short range attractive forces.
[45] To simplify notation, we leave out the parametric dependence of $g_2(\tau)$ on t and $\mathbf{r}$, which is however to be understood.
[46] Gravity compression is therefore much less relevant than for the 'creeping' depletion gels discussed in [8], made of particles with an almost 20 times larger buoyant mass.
[47] A. Duri, H. Bissig, V. Trappe, and L. Cipelletti, *Time-resolved-correlation measurements of temporally heterogeneous dynamics*, Phys. Rev. E **72**, 051401 (2005).
[48] Full correlation is never reached, arguably because of the fast internal relaxation modes of the gel that cause a 10% decay of the correlation functions over very short time.
[49] A series of unnormalized activity maps for other MQs is presented in the SM.
[50] Each correlation function has been obtained by averaging over the slack time between two MQs.
[51] H. Bissig, S. Romer, L. Cipelletti, V. Trappe, and P. Schurtenberger, *Intermittent dynamics and hyper-aging in dense colloidal gels*, PhysChemComm **6**, 21 (2003).
[52] From the data shown in the panel, this would happen when the gel is approximately two weeks old.
[53] L. Cipelletti, H. Bissig, V. Trappe, P. Ballesta, and S. Mazoyer, *Time-resolved correlation: A new tool for studying temporally heterogeneous dynamics*, J. Phys: Condens. Matt. **15**, S257 (2003).
[54] More precisely, to obtain a good statistics we considered a region of 50 ROIs centered on the blue one in Fig. 5.
[55] L. Buisson, S. Ciliberto, and A. Garcimartin, *Intermittent origin of the large violations of the fluctuation-dissipation relations in an aging polymer glass*, EPL **63**, 603 (2003).
[56] A. Crisanti and F. Ritort, *Intermittency of glassy relaxation and the emergence of a non-equilibrium spontaneous measure in the aging regime*, EPL **66**, 253 (2004).
[57] P. Sibani and H. J. Jensen, *Intermittency, aging and extremal fluctuations*, EPL **69**, 563 (2005).
[58] L. De Haan and A. Ferreira, *Extreme value theory: An introduction* (Springer Science & Business Media, 2007).
[59] R. A. Fisher and L. H. C. Tippett, *Limiting forms of the frequency distribution of the largest and smallest member of a sample*, Proc. Camb. Phil. Soc. **24**, 180 (1928).
[60] B. V. Gnedenko, *Sur la distribution limite du terme maximum d'une serie aleatoire*, Ann. Math. **44**, 423 (1943).
[61] J. Beirlant, Y. Goegebeur, J. Segers, and J. L. Teugels, *Statistics of extremes: Theory and applications* (John Wiley & Sons, 2006).
[62] The other two classes are the Fréchet–Pareto and the Weibull distributions.
[63] The dynamics in the jittery phase is not stationary, hence the statistical analysis was limited to a short time interval of 10^3 s, not too close to the moment when the next MQ takes place, in which the average value of the correlation index is approximately constant.
[64] E. A. Jagla, F. P. Landes, and A. Rosso, *Viscoelastic effects in avalanche dynamics: A key to earthquake statistics*, Phys. Rev. Lett. **112**, 174301 (2014).
[65] F. P. Landes, *Viscoelastic interfaces driven in disordered media: Applications to friction* (Springer, 2015).
[66] Y. Ogata, *Statistical model for standard seismicity and detection of anomalies by residual analysis*, Tectonophysics **169**, 159 (1989).
[67] S. Aime, L. Ramos, and L. Cipelletti, *Microscopic dynamics and failure precursors of a gel under mechanical load*, Proc. Natl. Acad. Sci. U. S. A. **115**, 3587 (2018).
[68] P. Bartlett, L. J. Teece, and M. A. Faers, *Sudden collapse of a colloidal gel*, Phys. Rev. E **85**, 021404 (2012).
[69] J.-P. Bouchaud and E. Pitard, *Anomalous dynamical light scattering in soft glassy gels*, Eur. Phys. J. E: Soft Matter Biol. Phys. **6**, 231 (2001).
[70] S. Buzzaccaro, E. Secchi, G. Brambilla, R. Piazza, and L. Cipelletti, *Equilibrium concentration profiles and sedimentation kinetics of colloidal gels under gravitational stress*, J. Phys.: Condens. Matter **24**, 284103 (2012).
[71] M. Jones, *Families of distributions arising from distributions of order statistics*, Test **13**, 1 (2004).
[72] M. Jones, *On a class of distributions with simple exponential tails*, Stat. Sinica , 1101 (2008).